Journal of Applied Polymer Science

Preparation and application of sulfadiazine surface molecularly imprinted polymers with temperature-responsive properties

Pengfei Ma,[1] Zhiping Zhou,[1] Wenming Yang,[1] Bingqing Tang,[2] Hong Liu,[3] Wanzhen Xu,[2] Weihong Huang[2]

[1]School of Materials Science and Engineering, Jiangsu University, Zhenjiang 212013, China
[2]School of Environment and Safety Engineering, Jiangsu University, Zhenjiang 212013, China
[3]Institute of Theoretical Chemistry, State Key Laboratory of Theoretical and Computational Chemistry, Jilin University, Changchun 130023, China
Correspondence to: Z. Zhou (E-mail: zhouzp@ujs.edu.cn) and W. Xu (E-mail: xwz09@ujs.edu.cn)

ABSTRACT: Novel, temperature-responsive molecularly imprinted polymers (TMIPs) based on potassium hexatitanate whiskers for selectively adsorbing sulfadiazine (SDZ) from aqueous media were prepared with methacrylic acid (MAA) and 4-vinylpyridine (4-VP) as cofunctional monomers and *N*-isopropyl acrylamide (NIPAM) as a temperature-responsive monomer. The template–monomer interactions were studied by molecular simulation. In particular, the effects of different kinds of crosslinkers on the selective recognition ability of the TMIPs in water media were investigated. The temperature–responsive adsorption performance and phase behavior of the molecularly imprinted polymers were studied by batch-mode binding experiments, swelling experiments, and contact angle testing. The results demonstrate that the combination of MAA, 4-VP, and NIPAM was a favorable temperature-responsive imprinted system for SDZ in water, and the cocrosslinking agent of ethylene glycol dimethacrylate (EGDMA) and *N*,*N*′-methylene bisacrylamide (MBA) was more suitable compared with either pure EGDMA or MBA. The adsorption kinetics and adsorption isotherms were analyzed by the fitting of different adsorption models. Also, the effect of the temperature on the recovery was investigated by the determination of the spiked SDZ in real-water samples with solid-phase extraction and high-performance liquid chromatography.
 J. Appl. Polym. Sci. **2015**, *132*, 41769.

KEYWORDS: adsorption; composites; hydrophilic polymers; swelling; theory and modeling

Received 17 August 2014; accepted 11 November 2014
DOI: 10.1002/app.41769

INTRODUCTION

Although antibiotics play an important role in treating infectious diseases, guaranteeing human health, and facilitating food industry development,[1,2] the excess use of antibiotics has begun to show negative effects. Its potential risks involve drug resistance and harm to body organs, which lead to double infection and cause social harm.[3,4] Recently, antibiotics, such as macrolides, sulfonamides, quinolones, and chloramphenicols, have been detected in our environment, including in wastewater from hospitals and sewage treatment plants, downstream water from farms, surface water, and underground water.[5–9] However, as the primary approach by which antibiotics enter the environment, sewage plants have not adopted technology for removing antibiotics in particular. A small portion of antibiotics eliminated in the sewage treatment is removed incidentally by traditional adsorbents, such as activated carbons, in the current process of sewage treatment.[9] Therefore, it is very necessary to develop a novel adsorbent with selectivity and practical value for industrial water treatment.

Molecular imprinting is a versatile and straightforward method for preparing artificial receptors that contain specific recognition sites for a given template molecule.[10] In recent years, molecularly imprinted polymers (MIPs) with different applications, such as solid-phase extraction (SPE),[11] drug delivery,[12] sensors,[13] and the mimicking of enzyme catalysis,[14] have been studied widely, and we've made great progress. In addition, the removal of pollutants or toxic substances in environment and industry is also an important application field for MIPs. Previously, we successfully prepared a series of imprinted adsorbents toward sulfides and nitrides in oil and investigated their application in oil desulfuration and denitrification.[15–17] Although studies of molecular imprinting have made great progress, some disadvantages exist in

Additional Supporting Information may be found in the online version of this article.

traditional MIPs that still need to be improved. Traditionally, MIPs suffer the drawbacks of highly rigid structures, slow mass transfer, incomplete template removal,[18,19] and unavailability in aqueous media.[20,21] In addition, we also expect to prepare MIPs that can achieve stimulus-responsive recognition behavior for a wider range of applications.[22]

To overcome the disadvantages of traditional MIPs, the surface molecular imprinting technique has been proven to be an effective method.[23,24] We improved adsorption performance of the MIPs prepared by surface molecular imprinting technique by decreasing the embedded recognition sites, reducing the transfer resistance, and accelerating the adsorption kinetics. To achieve stimulus-responsive recognition behavior in MIPs, *N*-isopropyl acrylamide (NIPAM) as a common temperature-responsive monomer has made a certain contribution to the molecular imprinting field.[22,25–30] MIPs synthesized with NIPAM as a temperature-responsive monomer exhibit a lower critical solution temperature (LCST; a critical temperature below which polymer is soluble, and above which phase separation of polymer solution occurs) in aqueous media. Swelling below the LCST and shrinking above the LCST of polymer changes the structure of the imprinted sites and helps one further realize temperature-responsive recognition behavior toward the template.

In this study, we chose sulfadiazine (SDZ), a sulfonamide that is used widely in the treatment of animals and humans but poses a risk of polluting the environment, as a template for further study in the field of molecular imprinting. In recent years, several MIPs toward sulfonamides have been prepared as stationary phase for high-performance liquid chromatography (HPLC) and as an SPE agent, and the applications mainly concentrate on the analysis and detection of sulfonamides, which exist in pork, chicken, fish, and poultry feed.[31–36] However, we also expected to prepare MIPs that could be applied well in aqueous media for determining sulfonamide contents in water samples or for removing sulfonamides in wastewater. Therefore, our aim was to design and prepare an MIP containing a favorable surface hydrophilicity, high selective adsorption ability, and controllable adsorption/desorption ability. According to the chosen template, SDZ, whose functional groups mainly contain aniline groups, sulfanilamido groups, pyrimidyl, methacrylic acid (MAA), and 4-vinylpyridine (4-VP), were selected as functional monomers. In the process of imprinting the assembly, SDZ formed an interaction force with MAA and 4-VP; it mainly depended on hydrogen bonding in organic media. However, the condition in the adsorption process was different. When MIPs are applied in aqueous media, the hydrogen-bond interactions become so weak that the hydrophobic interactions and electrostatic interactions (formed between alkaline pyrimidine group and acidic MAA) play a dominant role in the adsorption process. The crosslinker also plays an important role in the final performance of MIPs. The traditional crosslinker ethylene glycol dimethacrylate (EGDMA) has a structure of high rigidity and high hydrophobicity; however, the crosslinker *N*,*N*′-methylene bisacrylamide (MBA) has a relatively loose structure and satisfactory hydrophilicity. Different kinds of crosslinkers and different volumes of crosslinkers both had an effect on the adsorption performance of the resulting polymer materials.

In this article, we present a novel temperature-responsive molecularly imprinted polymer (TMIP) based on potassium hexatitanate whiskers. Before preparation, computer simulation and density functional theory (DFT) were used to calculate the binding energy between the template and monomer/crosslinker. The MIPs were synthesized with SDZ as a template molecule, 4-VP as a hydrophobic functional monomer, MAA as a negatively charged functional monomer, NIPAM as a temperature-responsive monomer, and MBA and/or EGDMA as crosslinkers (cf. Figure 1). To investigate the temperature-responsive behavior of the TMIPs and the influence of the crosslinker on the properties of the TMIPs, several groups of control experiments were designed and conducted. For the resulting materials, necessary characterization methods were used to determine the physical and chemical properties, and adsorption experiments were conducted to compare their adsorption performance. Furthermore, TMIPs with optimal performance coupled with SPE were used to determine SDZ in real-water samples at different temperatures.

EXPERIMENTAL

Materials

SDZ (99%), sulfamerazine (SMR; 99%), sulfamethazine (SMZ; 99%), sulfamethoxazole (SMO; 99%), MAA (99%) MBA (for electrophoresis, 99%) and NIPAM (98%) were purchased from Aladdin Reagent Co., Ltd. (Shanghai, China). 4-VP and EGDMA were supplied by Sigma-Aldrich Chemical Co. (St. Louis, MO). $K_2Ti_6O_{13}$ was procured by Shanghai Whisker Composite Material (Shanghai, China). 3-Methacryloxypropyl trimethoxysilane (MPS) and hydrochloric acid (37%) were received from Nanjing Chemical Reagent Co., Ltd. (Nanjing, China). Glacial acetic acid (HAc), azobisisobutyronitrile, acetonitrile, methanol, ethanol, and dichloromethane were obtained from Sinopharm Chemical Reagent Co., Ltd. (Shanghai, China). Methanol (for HPLC) was obtained from Tedia Co., Inc. (Ohio). All of the reagents were at least analytical-reagent grade and were used without further purification.

Molecular Simulation of the Binding Energy

Quantum chemical calculations applied in the computational simulation of molecular imprinting have attracted much attention in recent years.[37] The conformation, energy, and bonding information of interactional molecules were obtained to guide the MIP preparation and understand the imprinting mechanism through quantum chemical calculations. As one method of quantum chemical calculation, DFT, with its higher computational accuracy compared with the traditional Hartree–Fock method and faster computation speed compared with second-order Møller–Plesset theory, was used in this study. Template–monomer complexes with four different binding sites at a ratio of 1:1 were simulated. As shown in Figure 2, the binding sites of SDZ contained amidogen (site 1), imino groups (site 2), oxygen of sulfo groups (sites 3 and 6), and nitrogen of pyrimidine groups (sites 4 and 5). Because sites 2 and 5 interacted with the monomer simultaneously, they were regarded as one site. Either site 3 or site 6 was studied for space symmetry.

A server with an Intel Xeon E5–2620 CPU of 2.10 GHz, 16 GB of memory, a 64-bit Windows operating system, and Gaussian

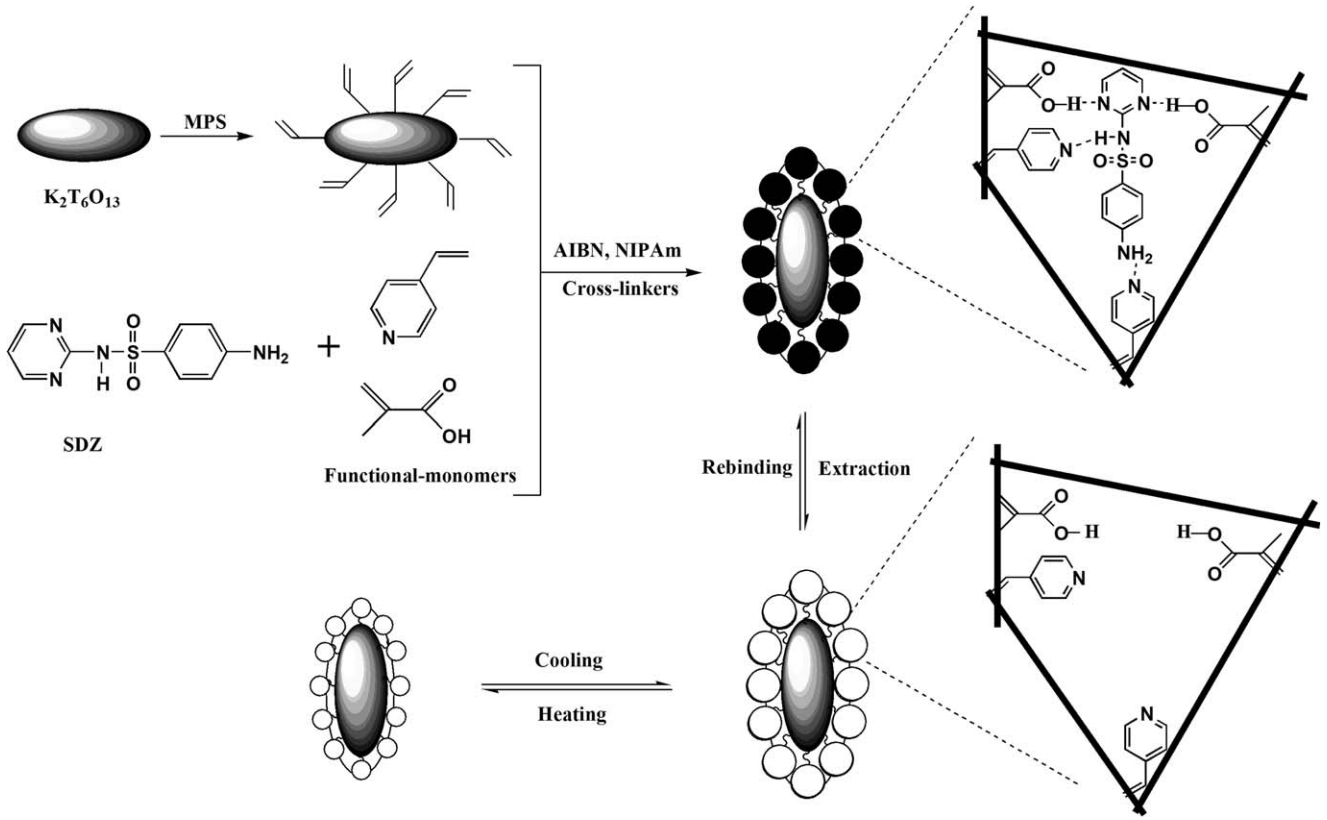

Figure 1. Schematic illustration of the preparation of the SDZ temperature-responsive imprinted polymer and the recognition process.

09 software was used to conduct the simulation. The job type was Opt + Freq. The method was set as restricted B3LYP of DFT in the ground state with the basis set of 6–311G (in quantum chemistry, the larger the scale of the basis set is, the higher the accuracy of the calculation is; 6–311G is one of the most common basis sets for meeting the requirements of accuracy). The molecular simulation was conducted *in vacuo*. First, the SDZ, monomers, and crosslinkers were optimized to obtain their conformations of minimum energy. The convergence criterion for confirming the calculation completion involved four aspects: a maximum force of less than 0.00045, a root mean square of maximum force of less than 0.0003, a maximum displacement of less than 0.0018, and a root mean square of maximum displacement of less than 0.0012. Second, the complexes of the SDZ and monomer/crosslinker were further optimized on the basis of the last step. Simultaneously, counterpoise correction was used to eliminate the basis set superposition error,[28] which had a nonignorable effect on the simulation results during intermolecular calculation. Finally, the binding energy (ΔE) between the SDZ and monomer/crosslinker was calculated with the following equation:

$$\Delta E = E_{complex} - E_{SDZ} - E_{monomer/crosslinker} + E_{BSSE} \quad (1)$$

where E_{SDZ} and $E_{monomer/crosslinker}$ are the energies of the SDZ and monomer/crosslinker (kJ/mol), respectively, in the minimum energy conformation; $E_{complex}$ represents the uncorrected energy of their complexes (kJ/mol); and E_{BSSE} is the energy of the basis set superposition error (kJ/mol).

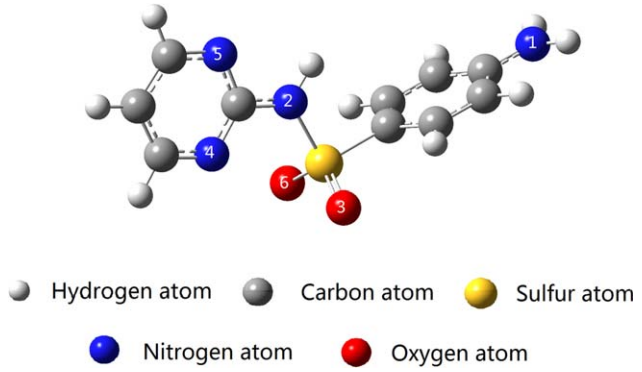

Figure 2. Possible binding sites of SDZ. [Color figure can be viewed in the online issue, which is available at www.interscience.wiley.com.]

Preparation of the Adsorbent

Preparation of the Vinyl-Modified $K_2Ti_6O_{13}$ Whiskers. First, $K_2Ti_6O_{13}$ whiskers were immersed in 3 mol/L HCl for 24 h to obtain the activated $K_2Ti_6O_{13}$. After suction filtration and washing to neutrality, the activated $K_2Ti_6O_{13}$ whiskers were dried in a vacuum-drying oven at 60°C until the quality was constant. Second, 0.5 g of MPS was added to the mixed solution of 2 mL of H_2O and 30 mL of ethanol. The HAc was added to the mixed solution drop by drop until its pH value was 1.5. The obtained mixed solution was set aside after 30 min of stirring. Then, 1 g of $K_2Ti_6O_{13}$, 100 mL of ethanol, and the hydrolysate of MPS were mixed in a three-necked flask with vigorous stirring. After the reaction continued for 4 h at 30°C, the product

Table I. Polymer Composition

Composition (mmol)	MIP1	NIP1	MIP2	NIP2	MIP3	NIP3	MIP4	NIP4
SDZ	1	—	1	—	1	—	1	—
MAA	2.67	2.67	2.67	2.67	2.67	2.67	2.67	2.67
4-VP	1.33	1.33	1.33	1.33	1.33	1.33	1.33	1.33
NIPAM	—	—	10	10	10	10	10	10
EGDMA	20	20	15	15	10	10	—	—
MBA	—	—	—	—	5	5	15	15

was centrifuged, washed repeatedly several times until the supernatant was neutral, and then dried in the vacuum-drying oven at 60°C until the quality was constant.

Preparation of the SDZ–MIPs and Non-Imprinted Polymers (NIPs) Based on $K_2Ti_6O_{13}$ Whiskers. The SDZ–MIPs and their corresponding NIPs were prepared with different formulas (cf. Table I) by the following surface molecular imprinting technique. First, the SDZ and functional monomers were dissolved in 30 mL of acetonitrile, and the mixture was put in a freezer for 12 h to obtain the preassembly solution. Second, the NIPAM and crosslinkers were added to 30 mL of acetonitrile by sonication for 10 min, and then, the preassembly solution was added to the mixture to obtain the prepolymerization solution. After purging with nitrogen for 10 min, 0.1 g of azobisisobutyronitrile was added to the reaction system as an initiator. The flask was sealed, and the mixture was polymerized according to the previous report: it was first prepolymerized at 50°C for 6 h, and then it was polymerized at 60°C for 24 h and further at 80°C for 6 h. After it was centrifuged and washed five times, the resulting MIPs were eluted with methanol–HAc (9:1 v/v) with Soxhlet extraction to remove the templates. Finally, the product was dried *in vacuo* at 60°C until the quality was constant. As a control, NIPs were synthesized by a similar method in the absence of SDZ.

Swelling Experiments

Swelling experiments were used to evaluate the phase-transition behavior of the adsorbent materials and to observe changes in their relative hydrophilicity/hydrophobicity at different temperatures. First, a certain quality of dried adsorbent sample packaged by filter paper was immersed in double-distilled water for 10 min. Also, single filter paper was immersed in a similar way. Then, the sample packaged by filter paper and the single filter paper were weighed, respectively, and the difference value between those was recorded as the wet weight of the samples (W_t). Subsequently, the soggy sample was dried in a vacuum oven until the quality was a constant (W_d). Finally, the swelling ratio was calculated with eq. (2). For each sample, the swelling experiment ran four times, and the average value was taken:

$$S=(W_t\text{-}W_d)/W_d \quad (2)$$

Characterization Methods

IR spectrophotometry with sample/potassium bromide (1:100–1:200) tableting was used to record the IR spectrogram ranging from 500 to 4000 cm^{-1}. The Nicolet Nexus 470 FTIR spectrometer used to record the FTIR spectra was supplied by Nicolet.

A sample in solid state on conductive tape attached to a copper billet after metal spraying was used to obtain the scanning electron microscopy (SEM) images. The S-4800 field emission SEM instrument used to observe the morphology of MIPs was purchased from Hitachi (Japan).

Thermogravimetric analysis data were obtained at a heating rate of 10°C/min from room temperature to 1000°C under an argon atmosphere. The Diamond TG/DTA instrument was supplied by PerkinElmer.

The test of the static water contact angle was used to evaluate the relative hydrophilicity/hydrophobicity of imprinted materials at 25 and 37°C.[38] Each sample was measured with a 2-μL drop of double-distilled water three times, and the average value was taken. A Krüss DSA25 contact angle measuring device was supplied by Krüss (Germany).

Adsorption Experiments

The adsorption experiments of the prepared adsorption materials included adsorption kinetics, adsorption isotherms, adsorption selectivity, and adsorption responsiveness; the tests were performed in batch mode to confirm the experimental parameters, including the adsorption time and temperature, and to evaluate the adsorption performances of different imprinted materials. SDZ aqueous solutions with concentrations ranging from 1 to 20 μg/mL and mixed solutions of SDZ and its analogues (10 μg/mL) were prepared. The volume of the adsorbate solution used for the adsorption experiments was confirmed to be 7 mL according to the mass of adsorbent (10 mg) by volume optimization. The concentrations of the adsorbate solutions after adsorption were determined by HPLC (Shimadzu 2010A, Japan). Methanol–H_2O–HAc (30/70/0.1 v/v/v) was selected as the mobile phase and the column ran at a flow rate of 1.0 mL/min. In addition, to further study the temperature-responsive behavior of TMIP, a test of temperature-responsive behavior was conducted. The adsorption capacities of the adsorbent materials were measured as the temperature increased from 20 to 65°C.

SPE Experiments

The MIP that was demonstrated to possess the best adsorption performance by previously adsorption experiments was used as an SPE adsorbent to determine the SDZ content in real-water

Table II. Binding Energies of the SDZ–Monomer/Crosslinker Complex

Monomer/crosslinker	Binding site	E_{SDZ} (au)	$E_{monomer/crosslinker}$ (au)	$E_{complex}$ (au)	E_{BSSE} (au)	ΔE (au)	ΔE (kJ/mol)
4-VP	1	−1154.4903	−325.6699	−1480.171	0.002522	−0.01334	−35.04
	2	−1154.4903	−325.6699	−1480.169	0.004189	−0.01397	−36.67
AM	1	−1154.4903	−247.2919	−1401.791	0.003647	−0.01308	−34.35
	2	−1154.4903	−247.2919	−1401.798	0.004837	−0.02167	−58.89
	3	−1154.4903	−247.2919	−1401.794	0.003955	−0.01638	−43.01
	4	−1154.4903	−247.2919	−1401.796	0.003889	−0.01822	−47.84
MAA	1	−1154.4903	−306.4711	−1460.969	0.004379	−0.01207	−31.68
	2	−1154.4903	−306.4711	−1460.983	0.005733	−0.02771	−72.74
	3	−1154.4903	−306.4711	−1460.975	0.005027	−0.01891	−49.66
	4	−1154.4903	−306.4711	−1460.972	0.004135	−0.01527	−40.09
NIPAM	1	−1154.4903	−365.2251	−1519.724	0.003251	−0.01249	−32.79
	2	−1154.4903	−365.2251	−1519.725	0.003033	−0.00965	−25.34
	3	−1154.4903	−365.2251	−1519.72	0.004956	−0.01276	−33.51
	4	−1154.4903	−365.2251	−1519.721	0.003785	−0.01001	−26.28
EGDMA	—	−1154.4903	−690.3111	−1844.824	0.006328	−0.02922	−76.72
MBA	—	−1154.4903	−532.6879	−1687.185	0.006295	−0.01345	−35.32

samples at different temperatures (25, 35, and 45°C) to study the effect of the temperature on the experimental recovery and to validate its potential applications. The tap water and water obtained from the Yangtze River were used as real water for this study. The water was spiked with SDZ, and the spiking concentrations were 0.01, 0.1, and 1 μg/mL. An HGC-8 digital controlled SPE device (Shanghai Hegong Science and Technology Co., Ltd., China) was used to conduct the recovery experiment at a flow rate of 0.5 mL/min. First, 0.5 g of adsorbent material between two sieve plates was placed into an empty SPE cartridge (9 mm in internal diameter, 64 mm in length). Before the spiked water sample was loaded, the cartridge was successively preconditioned with 5 mL of methanol and 10 mL of double-distilled water. After that, the spiked water sample was loaded into the cartridge. Then, the cartridge was washed with 5 mL of double-distilled water and 5 mL of dichloromethane and eluted twice with 10 mL of a methanol/acetic mixed solution (9:1 v/v). The eluents were collected and dried under a nitrogen stream, and the residues were dissolved in 2 mL of double-distilled water in a renewable manner. Finally, the spiked water samples after selective enrichment were determined by HPLC, and the enrichment coefficient was 25. The previous conditions of the washing step refer to the previous literature[39] and were further optimized.

RESULTS AND DISCUSSION

Analysis of the Binding Energy

The conformations and binding energies of the SDZ–monomer/crosslinker complex are shown in Figure S1–S5 in the Supporting Information and Table II, respectively. For binding site 1 of SDZ, 4-VP (−35.04 kJ/mol) formed stronger hydrogen-bond interactions with SDZ than acrylamide (AM) (−34.35 kJ/mol), MAA (−31.68 kJ/mol), and NIPAM (−32.79 kJ/mol), but its superiority was not obvious. For binding sites 2 and 3, MAA showed a distinct advantage in the hydrogen-bond interaction formation (−72.74 and −49.66 kJ/mol). In addition, AM showed better performance for binding site 4 (−47.84 kJ/mol). Therefore, it was hard for NIPAM to form an interaction force with SDZ in the presence of a common functional monomer. We needed its function to exist in the network of the MIPs and to make the polymer swell or shrink according to temperature conditions; this was in accordance with previous works.[40,41] In view of the strong interaction force formed between the MAA and pyrimidine groups, MAA was selected as the functional monomer toward SDZ. In addition, 4-VP, which could form interaction forces with amidogen, was also used as a cofunctional monomer to provide hydrophobic interactions in the process of adsorption. The binding energy of SDZ and MBA (−35.32 kJ/mol) was too low to interfere with the stabilized complex formed from the template and monomers. The binding energy of SDZ and EGDMA reached −76.72 kJ/mol and was contributed by two hydrogen-bond interactions. In consideration of its steric hindrance, it was also hard for EDGMA to occupy the position of MAA or 4-VP in the SDZ–monomer complex.

Characterizations

Swelling Experiments. Swelling experiments were used to understand the phase behavior and the relative hydrophilicity of the prepared imprinted materials. Figure 3 presents the swelling ratio curves of four kinds of imprinted adsorbents. As the temperature improved, the swelling ratios of MIP2, MIP3, and MIP4 all exhibited a dramatic decline versus the inactivity of MIP1. The phase-transition behaviors of the imprinted materials responsive to temperature were attributed to the presence of NIPAM. For the three kinds of TMIPs, the swelling ratios were ranked in descending order: MIP4 > MIP3 > MIP2; this showed that MIP4 possessed the highest hydrophilicity, and the hydrophilicity of MIP3 was higher than that of MIP2. Their differences in the hydrophilicity resulted from the volumes of the

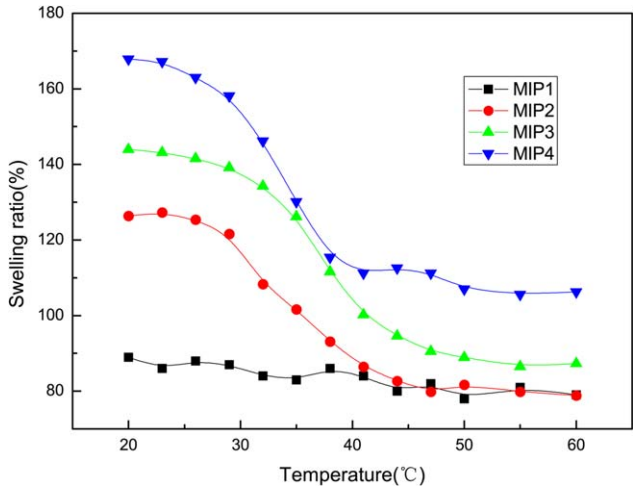

Figure 3. Swelling ratio curves of the prepared adsorption materials. [Color figure can be viewed in the online issue, which is available at www.interscience.wiley.com.]

hydrophilic crosslinker MBA. In a comparison of MIP2 and MIP3, the addition of MBA improved the hydrophilicity of the materials. The obvious phase-transition behavior occurred mainly from 30 to 40°C; this was consistent with the LCST of polyNIPAM (32°C).

Test of the Static Water Contact Angle. Figure 4 presents the images of the static water contact angles of imprinted materials, including MIP1, MIP2, MIP3, and MIP4 at 25 and 37°C. Obvious changes in the static water contact angles were observed for MIP2, MIP3, and MIP4 from 25 to 37°C; this showed that NIPAM successfully changed the hydrophilicity with shifting temperatures. Also, MIP3 possessed improved the hydrophilicity compared with MIP2, but its hydrophilicity was lower than that of MIP4. The appropriate addition of MBA as a crosslinker effectively improved the hydrophilicity of the imprinted material because of the excellent hydrophilicity of poly(*N*,*N*′-methylene bisacrylamide).

Other Characterizations. Other characterizations, including IR spectroscopy, SEM, and thermogravimetry, and their analyses are shown in the Supporting Information (Figures S6–S7).

Evaluation of the Adsorption Performance

The evaluation criteria of the adsorption performance included the equilibrium adsorption capacity (q_e; mg/g) and adsorption selectivity; these were applied to confirm the MIP with optimum adsorption performance. The equilibrium adsorption capacity was calculated with eq. (3), and the adsorption selectivity, including the distribution coefficient (K_d, mL/g), selectivity coefficient (K), and relative selectivity coefficient (K'), of SDZ and its analogues were calculated by eqs. (4–6):

$$q_e = (C_0 - C_e)V/m \tag{3}$$

where q_e represents the equilibrium adsorption ability of the adsorbent (mg/g); C_0 and C_e are the concentrations of the adsorbate at the initial time and at equilibrium, respectively (mg/L); V is the solution volume (L); and m is the weight of adsorbent (g):

$$K_d = q_e/C_e \tag{4}$$

$$K = K_d(\mathrm{SDZ})/K_d(X) \tag{5}$$

$$K' = K_{\mathrm{MIP}}/K_{\mathrm{NIP}} \tag{6}$$

where K_{MIP} represents the selectivity coefficient of MIP; K_{NIP} is the selectivity coefficient of NIP; and X is the analogues of SDZ.

Figure 5 presents the adsorption capacity (equilibrium adsorption state; concentration of SDZ aqueous solution = 10 μg/mL) of various groups of adsorbent materials at temperatures of 25, 35, and 45°C. The adsorption capacities of the imprinted materials were all much higher than those of the nonimprinted

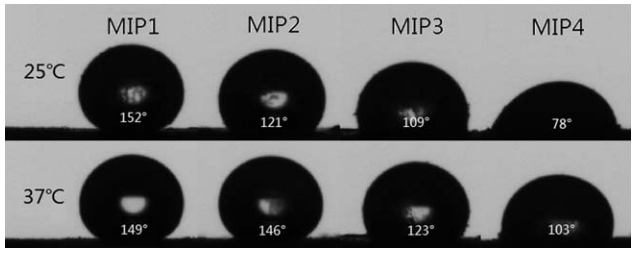

Figure 4. Images of the static water contact angles of the prepared imprinted materials at 25 and 37°C.

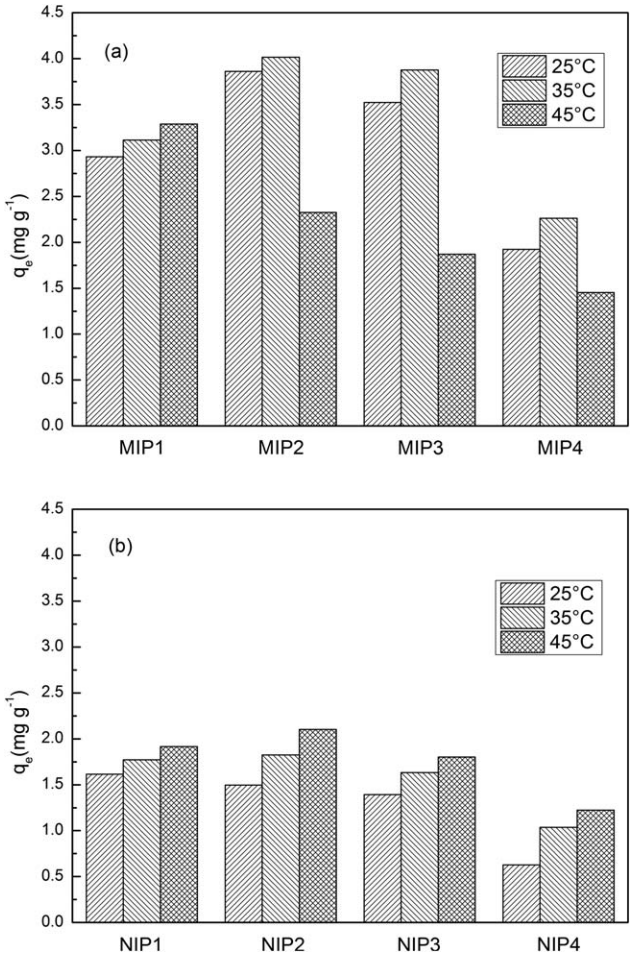

Figure 5. Adsorption capacity of various groups of adsorbent material at 25, 35, and 45°C.

Table III. Specific Binding of the MIPs and NIPs Toward SDZ at 35°C

		MIP			NIP			
Number	Sulfonamide	q_e (mg/g)	K_d (L/g)	K	q_e (mg/g)	K_d (L/g)	K	K'
1	SDZ	2.234	0.328	—	0.845	0.0961	—	
	SMR	1.351	0.167	1.965	0.884	0.101	0.951	2.07
	SMZ	1.337	0.165	1.988	0.945	0.109	0.882	2.25
	SMO	0.615	0.0674	4.866	0.506	0.0594	1.617	3.01
2	SDZ	2.568	0.406	—	0.878	0.101	—	
	SMR	1.285	0.157	2.586	0.811	0.0917	1.101	2.35
	SMZ	1.113	0.132	3.076	0.792	0.0893	1.131	2.72
	SMO	0.403	0.0427	9.508	0.368	0.0388	2.603	3.65
3	SDZ	2.912	0.542	—	0.831	0.0943	—	
	SMR	1.381	0.172	3.151	0.726	0.081	1.116	2.82
	SMZ	1.146	0.137	3.956	0.673	0.0745	1.266	3.12
	SMO	0.315	0.033	16.424	0.257	0.0267	3.532	4.65
4	SDZ	1.467	0.186	—	0.485	0.0521	—	
	SMR	1.065	0.126	1.476	0.374	0.0395	1.319	1.12
	SMZ	0.955	0.111	1.676	0.438	0.0467	1.116	1.51
	SMO	0.663	0.0732	2.541	0.427	0.0455	1.145	2.22

materials; this demonstrated that the imprinted materials were successfully prepared with imprinted binding sites. The maximum adsorption capacities of the MIPs were ranked in descending order: MIP2 > MIP3 > MIP1 > MIP4. MIP2 possessed the highest adsorption capacity, and MIP3 ranked second in minor disadvantage. The poor recognition capacity of the MIP4 adsorbent material toward SDZ was attributed to the loose structure, which resulted from the use of only MBA as a crosslinker. Therefore, single MBA as the crosslinker was not suitable for the preparation of efficient MIPs for SDZ. The adsorption capacities of MIP2, MIP3, and MIP4 all achieved the maximum values at about 35°C and decreased at about 45°C. However, the MIP1 without the addition of NIPAM did not exhibit this change because of the absence of NIPAM. This indicated that both tight and loose spatial structures affected the recognition ability of the imprinted sites. This result demonstrates that the MIPs with temperature-responsive behaviors were successfully prepared by the addition of NIPAM as a temperature-responsive monomer. The falling extents of MIP2, MIP3, and MIP4 from 35 to 45°C were 42.1, 51.8, and 35.8%, respectively. Obviously, MIP3 had the most considerable temperature-responsive ability.

Table III presents the experimental result of the adsorption selectivity at 35°C, the temperature at which TMIPs showed the largest adsorption capacity. We observed that all of the imprinted materials possessed selective adsorption ability, and MIP3 possessed the maximum adsorption capacity toward SDZ in mixed aqueous solution. The K' values of MIP1 toward the three analogues were 2.07, 2.25 and 3.01, respectively; this demonstrated the availability of ordinary MIP for SDZ with 4-VP and MAA as cofunctional monomers. With the addition of a temperature-responsive monomer (NIPAM), MIP2 happened to exhibit enhanced the selective adsorption ability. The reason may have been that NIPAM exhibited favorable water solubility at 35°C, and the surface hydrophilicity of the imprinted material was enhanced. Moreover, MIP3 with EGDMA and MBA as cocrosslinkers exhibited the optimal adsorption selectivity, but MIP4 with MBA as a single crosslinker showed poor adsorption selectivity performance. This illustrated that appropriate volumes of MBA could effectively reduce nonspecific adsorption through the improvement of the surface hydrophilicity. However, an excess of MBA led to a decrease in the adsorption selectivity and even the unavailability of imprinted recognition sites; this was attributed to the too-loose structure, which could not meet the requirement of imprinted sites.

On the basis of the previous analysis, MIP3, with NIPAM as a temperature-responsive monomer and EGDMA and MBA as cocrosslinkers, possessed the most favorable temperature-responsive recognition behavior and the best adsorption selectivity. MIP3 could be the optimal imprinted adsorbent for our future studies.

Temperature-Responsive Recognition Behavior of the Imprinted Material

Figure 6 presents the temperature-responsive recognition behavior of MIP3, which showed the best adsorption performance in our study, and the behavior of NIP3. We defined the maximum adsorption capacity of both MIP3 and NIP3 in the process of temperature change as 100% binding. At the initial temperature (20°C), MIP3 adsorbed about 80% SDZ compared with the maximum adsorption capacity in the whole experimental process. As the temperature rose, MIP3 further adsorbed SDZ existing in the solution environment, and the adsorption capacity achieved the maximum value at about 35°C, which was

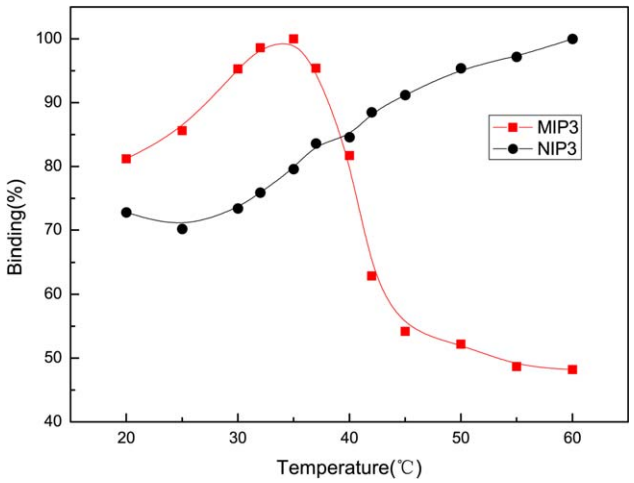

Figure 6. Temperature-responsive recognition behavior of MIP3 and NIP3. (The ordinate value represents the relative value of MIP3 and NIP3, respectively compared with the maximum adsorption during the whole process of temperature variation). [Color figure can be viewed in the online issue, which is available at www.interscience.wiley.com.]

near the LCST of NIPAM. As the temperature increased further, the adsorption capacity underwent a rapid decline from 35 to 45°C. The adsorption capacity decreased further slowly until it stabilized around 55°C. Before the LCST, the relatively loose structure of the imprinted sites caused the recognition ability to not be able to achieve its maximum. When temperature increased higher than LCST, the binding ability decreased sharply; this could be attributed to the structural shrinkage of the imprinted sites. Both tight and loose spatial structures of the imprinted sites led to the decrease in the recognition ability. For NIP3, the adsorption capacity increased slowly as the temperature rose. The considerable temperature-responsive recognition behavior of MIP3 was consistent with previous work on TMIPs toward another SMZ with a similar reaction environment (mainly the solvent and reaction temperature) during the grafting polymerization;[26] also, it further demonstrated its availability and reasonability for the following study on its properties and applications.

Analysis of the Adsorption Kinetics

Adsorption kinetics was used to obtain the exact adsorption equilibrium time and to understand the adsorption mechanism to some extent. In this research, adsorption processes at temperatures of 25, 35, and 45°C in particular were studied for MIP3 with the optimal adsorption performance and its corresponding NIP (NIP3). The experimental data of adsorption kinetics were fit with a pseudo-first-order kinetics model, a pseudo-second-order kinetics model, and an Elovich kinetics model. The three kinds of kinetics models were expressed by the following equations, respectively:[42–44]

$$q_t = q_e(1-e^{-k_1 t}) \quad (7)$$

$$q_t = q_e^2 k_2 t/(1+q_e k_2 t) \quad (8)$$

$$q_t = (1/b)\ln(ab)+(1/b)\ln(t) \quad (9)$$

where q_e and q_t are the amounts of adsorbed SDZ at equilibrium and time t, respectively; t is the adsorption time; k_1 and k_2 are the adsorption rate constants of the pseudo-first-order and pseudo-second-order, respectively; a represents the initial adsorption rate; and b is a constant related to the surface coverage.

The fitting curves and the fitting data of kinetics models of MIP3 and NIP3 are shown in Table IV and Figure 7, respectively. According to Figure 7(a), it was obvious that MIP3 at 25 and 35°C fit the pseudo-second-order kinetics model well, but MIP3 at 45°C fit the pseudo-first-order kinetics model well. At the initial adsorption stage, the q_t value grew rapidly (approaching linear adsorption). As time went on, the growth rate of q_t became slow, and the q_t value of MIP3 at different temperatures increased until the adsorption process achieved equilibrium (nonlinear adsorption). Before equilibrium, the adsorption time of MIP3 at 25 and 35°C was distinctly longer than that of MIP3 at 45°C. All of the previous results reflect the fundamental difference of the adsorption mechanisms between MIP3 at 25 and 35°C and MIP3 at 45°C. The linear adsorption stage

Table IV. Kinetic Parameters of MIP3 and NIP3 Toward SDZ

		MIP3			NIP3		
		298 K	308 K	318 K	298 K	308 K	318 K
Kinetic model	$q_{e,exp}$ (mg/g)	3.524	3.874	1.874	1.388	1.634	1.808
Pseudo-first-order	$q_{e,cal}$ (mg/g)	3.424	3.784	1.87	1.389	1.623	1.794
	k_1 (min^{-1})	0.254	0.246	0.238	0.276	0.349	0.425
	R^2	0.9179	0.9343	0.9835	0.9931	0.997	0.9907
Pseudo-second-order	$q_{e,cal}$ (mg/g)	3.613	3.987	1.972	1.462	1.702	1.874
	k_2 (mg g^{-1} min^{-1})	0.121	0.108	0.206	0.317	0.336	0.373
	R^2	0.9912	0.9911	0.9713	0.9725	0.9679	0.9726
Elovich	a (mg g^{-1} min^{-1})	12.83	13.874	5.724	5.746	12.839	32.594
	b (g/mg)	2.119	1.916	3.782	5.315	4.973	5.002
	R^2	0.8986	0.8834	0.7928	0.7594	0.7117	0.6947

$q_{e,exp}$, adsorption capacity obtained by experiment; $q_{e,cal}$, adsorption capacity obtained by model fitting.

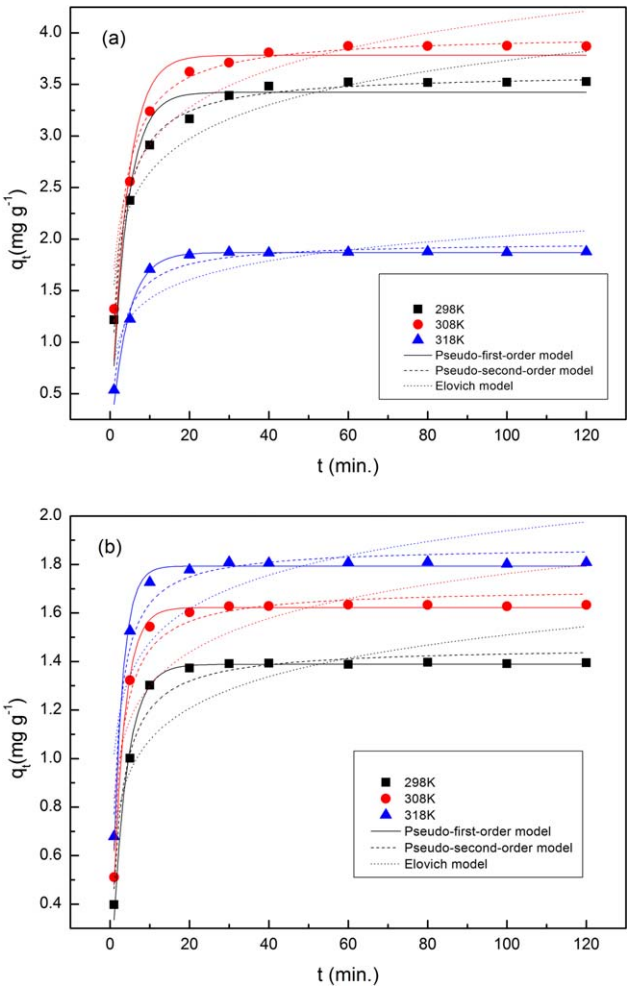

Figure 7. Adsorption kinetics of (a) MIP3 and (b) NIP3 at 298, 308, and 318 K. [Color figure can be viewed in the online issue, which is available at www.interscience.wiley.com.]

mainly involved surface diffusion, whereas the nonlinear adsorption mainly involved intraparticle diffusion. The much longer stages of the nonlinear adsorption of MIP3 at 25 and 35°C compared with those of MIP3 at 45°C and NIP3 at 25, 35, and 45°C could commendably explain the availability of MIP3′ imprinted recognition sites at 25 and 35°C. When the temperature rose to 45°C, the intraparticle diffusion of MIP3 became weaker on account of the shrinkage and invalidation of imprinted sites. The correlation coefficient (R^2) of the pseudo-second-order kinetics of MIP3 at 25 and 35°C were all above 0.99 (at 0.9912 and 0.9911, respectively); however, the R^2 of the pseudo-second-order kinetics of MIP3 at 45°C (at 0.9713) was lower than that of the pseudo-first-order kinetics (0.9835). The R^2 values of the pseudo-first-order kinetics of MIP3 at 25, 35, and 45°C were all above 0.99 (at 0.9931, 0.997, and 0.9907, respectively).

Analysis of the Adsorption Isotherms

The adsorption properties of the adsorbent materials were depicted by the fitting of the data of the adsorption isotherms. Three adsorption isotherms models, the Langmuir, Freundlich, and Sips models, were selected, and they are expressed by the following equations, respectively:[45–47]

$$q_e = q_{mL} k_L C_e / (1 + k_L C_e) \quad (10)$$

$$q_e = k_F C_e^{1/n_F} \quad (11)$$

$$q_e = [q_{ms} (a_s C_e)^{1/n_s}] / [1 + (a_s C_e)^{1/n_s}] \quad (12)$$

where q_{mL} is the maximum adsorption capacity of monolayer adsorption; k_L is the Langmuir constant (L/mg); k_F and n_F are the Freundlich constants representing the adsorption capacity and intensity, respectively; a_s is a constant related to the adsorption energy; and n_s is used to express the uniformity of adsorption. The Langmuir and Freundlich models are common adsorption isotherms models for describing the adsorption process, and the Sips model is generally used to describe nonuniform surface adsorption.

Figure 8 and Table V present the fitting curves and fitting data, respectively, of the adsorption isotherms of MIP3 and NIP3. As shown in Figure 8, the equilibrium adsorption capacities at different temperatures increased with decreasing slope as the

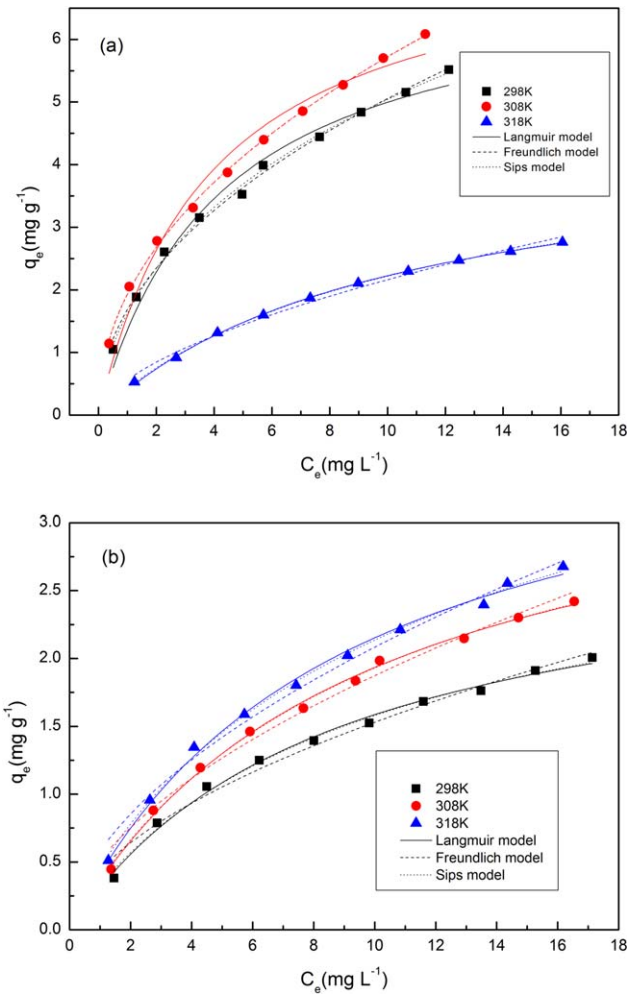

Figure 8. Adsorption isotherms of (a) MIP3 and (b) NIP3 at 298, 308, and 318 K. [Color figure can be viewed in the online issue, which is available at www.interscience.wiley.com.]

Table V. Adsorption Isothermal Parameters of MIP3 and NIP3 Toward SDZ

		MIP3			NIP3		
Isotherm model		298 K	308 K	318 K	298 K	308 K	318 K
Langmuir	k_L (L/mg)	0.238	0.257	0.0985	0.117	0.105	0.113
	q_{mL} (mg/g)	7.098	7.752	4.488	2.945	3.779	4.052
	R^2	0.9801	0.9666	0.9993	0.9937	0.9972	0.9956
Freundlich	k_F	1.6886	1.9324	0.5647	0.442	0.509	0.581
	n_F	2.099	2.121	1.715	1.855	1.767	1.804
	R^2	0.9955	0.999	0.9901	0.9819	0.9852	0.9887
Sips	q_{ms} (mg/g)	18.21	188.078	4.892	3.161	3.972	4.818
	a_s	0.0197	7.523	0.082	0.0999	0.0943	0.0772
	n_s	1.691	2.078	1.064	1.062	1.04	1.136
	R^2	0.9966	0.9988	0.9995	0.993	0.9969	0.9961

q_{ms}, a constant related to the adsorption capacity in Eq.12.

equilibrium concentrations of SDZ increased. The six isotherms curves were ranked in descending order: MIP3 at 308 K > MIP3 at 298 K > MIP3 at 318 K > NIP3 at 318 K > NIP3 at 308 K > NIP3 at 298 K; this was in accordance with the previous results. MIP3 at 298 and 308 K all exhibited excellent adsorption capacities compared with NIP3. Moreover, MIP3 showed a favorable stimuli-responsive recognition ability that relied on the change in temperature. The q_e value of MIP3 at 308 K was at least double of that of MIP3 at 318 K. In addition, the trend and degree of the curve of MIP3 at 318 K was similar to that of NIP3 at 318 K; this indicated that MIP3 at 318 K lost the function of the imprinted recognition sites to a great extent. As shown in Table V, all of the R^2 values of the Freundlich models of MIP3 and the Langmuir models of NIP3 at the three temperatures were above 0.99. Overall, MIP3 fit the Freundlich model well, and NIP3 fit the Langmuir model well. However, the special case was MIP3 at 318 K. Although the R^2 value of the Freundlich model of MIP3 at 318 K attained a value of 0.9901, the R^2 of the Langmuir model was higher than that (at 0.9993). The differences in the fitting results reflected the differences in the adsorption mechanisms that resulted from imprinted sites that were or were not available. Moreover, both MIP3 and NIP3 at different temperatures fit the Sips model well; the Sips model combines the Langmuir and Freundlich models. In the Sips equation, the closer to 1 the n_s value is, the more uniform the surface of the adsorbent is. So, both MIP3 and NIP3 were provided with considerable uniformity of adsorption. Because the nonimprinted materials did not involve intraparticle diffusion, it was easy to understand that the n_s value of NIP3 was closer to 1 than that of MIP3.

Determination of SDZ in the Real-Water Samples

The feasibility of using the prepared TMIP as SPE adsorbents for the selective enrichment and determination of SDZ in real water was examined.[48] In recovery experiments, we focused on and investigated the temperature effect on experimental recovery. By adjusting different temperatures, we could control the selectivity and adsorption ability of TMIP; this further changed the results of recovery. As visual representations of the effect of using TMIP as SPE adsorbents, the chromatograms of a blank Yangtze River sample, a sample spiked with SDZ at a concentration of 0.01 μg/mL, and a spiked sample after selective extraction and enrichment with MIP3 at 25, 35, and 45°C are shown in Figure 9, respectively. In a comparison of Figures 9(a) and 9(b), there was no obvious peak of SDZ after the Yangtze River sample was spiked with SDZ because the limit of detection of SDZ in the original spiked sample was so large for the concentration of 0.01 μg/mL SDZ. Figure 9(c,e,d) presents the available peaks of SDZ distinctly after selective extraction and enrichment with MIP3 as an SPE adsorbent at 25, 35, and 45°C, respectively. The peak areas of irrelevant compounds were obviously smaller, the base line of the chromatogram was smoother, and

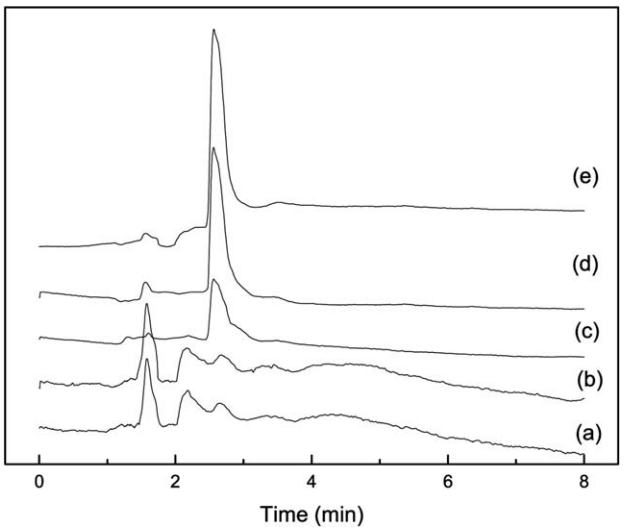

Figure 9. HPLC chromatograms of the blank Yangtze River sample and Yangtze River sample spiked with SDZ at a concentration of 0.01 μg/mL before and after extraction and enrichment through the MIP3-packed SPE cartridges at 25, 35, and 45°C: (a) blank Yangtze River sample, (b) spiked Yangtze River sample, and spiked Yangtze River sample after extraction and enrichment through MIP3 at (c) 25, (d) 45, and (e) 35°C.

Table VI. Recoveries of SDZ from Spiked Real-Water Samples

	Sample											
	0.01 μg/mL				0.1 μg/mL				1 μg/mL			
	Tap water		Yangtze River		Tap water		Yangtze River		Tap water		Yangtze River	
Temperature (°C)	Recovery (%)	RSD (%)	Recovery (%)	RSD (%)	Recovery (%)	RSD (%)	Recovery (%)	RSD (%)	Recovery (%)	RSD (%)	Recovery (%)	RSD (%)
25	44.5	6.7	51.5	5.8	51.6	6.1	50.3	6.2	55.8	3.4	50.5	4.4
35	74.9	5.8	94.3	7.5	87.4	5.6	84.5	3.5	93.4	4.1	89.2	6.0
45	36.7	4.3	29.7	5.2	31.4	4.1	32.4	2.7	23.6	3.7	21.2	3.1

$n = 6$.

the limit of detection was lower. Because of the different experimental conditions of temperature, the peak areas varied in size. Compared with 25 and 45°C, 35°C was the optimum temperature for obtaining the highest recovery.

To evaluate the application and the accuracy of the developed method, tap-water samples and Yangtze River samples spiked with three levels of SDZ including 0.01, 0.1 and 1 μg/mL were researched. Table VI presents the whole data of recoveries and corresponding relative standard deviations (RSDs), including tap-water and Yangtze River samples, with spiked SDZ at 25, 35, and 45°C. All the data of recoveries were averaged after six measurements. The mean recoveries of the tap-water and Yangtze River samples with MIP3 as the SPE packing at 35°C ranged from 74.9 to 93.4% and from 84.5% to 94.3%, respectively. The RSDs were less than 7.5%. When SPE was conducted under 45°C, the recoveries dropped to less than 37%. The dramatic change in the recovery at different temperatures demonstrated that the recovery of SDZ from real-water samples was temperature-dependent. All of the results revealed that TMIP could be applied to the selective extraction, enrichment, and determination of SDZ in real-water samples.

CONCLUSIONS

In this study, various kinds of TMIPs based on potassium hexatitanate whiskers were prepared to achieve the controllable adsorption/desorption of SDZ in water. The combination of MAA, 4-VP, and NIPAM was validated to be an effective temperature-responsive imprinted system for SDZ. The kind of crosslinker used during the polymerization was found to play an important role in the temperature-responsive behavior and selective adsorption ability of the prepared TMIPs. Pure EGDMA led to a highly rigid structure and nonspecific adsorption, but the excessively loose structure of pure MBA resulted in the invalidation of imprinted sites to a large extent. EGDMA-*co*-MBA was proven to be more suitable for use as a crosslinker compared with pure EGDMA or MBA in our study. By adjusting the external temperature, we realized the controllable adsorption/desorption of SDZ in aqueous media. The adsorption kinetics of TMIP with EGDMA-*co*-MBA as a crosslinker at 298 and 308 K fit the pseudo-second-order kinetics model well versus the good fitting of the pseudo-first-order kinetics model for that at 318 K. The adsorption isotherms at 298 and 308 K fit the Freundlich model well, but the adsorption isotherms at 318 K fit the Langmuir model better than Freundlich model. The differences in the adsorption mechanism at different temperatures explained the temperature-responsive behavior from another side. As an important application of MIPs, the recoveries at different temperatures with the combination of SPE and HPLC were investigated. Recoveries ranging from 74.9 to 94.3% and RSDs of less than 7.5% were desirable. The recovery of SDZ from real water was temperature-dependent, and the prepared TMIP could be applied to the selective enrichment and determination of SDZ in real-water samples.

ACKNOWLEDGMENTS

This work was supported by the National Basic Research Program of China (973 Program, contract grant number 2012CB821500), National Natural Science Fund (contract grant numbers 21106056 and 21174057), Jiangsu Natural Science Foundation of China (contract grant number BK2011512), and Senior Talent Foundation of Jiangsu University (contract grant number 14JDG057).

REFERENCES

1. Singer, R. S.; Finch, R.; Wegener, H. C.; Bywater, R.; Walters, J.; Lipsitch, M. *Lancet Infect. Dis.* **2003**, *3*, 47.
2. Cabello, F. C. *Environ. Microbiol.* **2006**, *8*, 1137.
3. Martinez, J. L. *Environ. Pollut.* **2009**, *157*, 2893.
4. Du, L. F.; Liu, W. K. *Agron. Sustain. Dev.* **2012**, *32*, 309.
5. Middleton, J. H.; Salierno, J. D. *Ecotox. Environ. Safe.* **2013**, *88*, 79.
6. Edge, T. A.; Hill, S. *J. Microbiol.* **2005**, *51*, 501.
7. Yasojima, M.; Nakada, N.; Komori, K.; Suzuki, Y.; Tanaka, H. *Water Sci. Technol.* **2006**, *53*, 227.
8. Hruska, K.; Franek, M. *Vet. Med.-Czech.* **2012**, *57*, 1.
9. Xu, W. H.; Zhang, G.; Li, X. D.; Zou, S. C.; Li, P.; Li, Z. H.; Li, J. *Water Res.* **2007**, *41*, 4526.
10. Whitcombe, M. J.; Vulfson, E. N. *Adv. Mater.* **2001**, *13*, 467.
11. Tamayo, F. G.; Turiel, E.; Martin-Esteban, A. *J. Chromatogr. A* **2007**, *1152*, 32.
12. Puoci, F.; Cirillo, G.; Curcio, M.; Curcio, O. I.; Iemma, F.; Picci, N. *Expert Opin. Drug Del.* **2011**, *8*, 1379.
13. Haupt, K. Mosbach, K. *Chem. Rev.* **2000**, *100*, 2495.

14. Resmini, M. *Anal. Bioanal. Chem.* **2012**, *402*, 3021.
15. Li, H.; Li, W. Z.; Wang, N. W.; Ma, X. H.; Niu, D. D.; Jiang, B.; Liu, L. K.; Liu, W. H.; Yang, W. M.; Zhou, Z. P. *Microchim. Acta* **2012**, *179*, 123.
16. Cao, Y.; Liu, L. K.; Xu, W. Z.; Wu, X. Y.; Huang, W. H. *J. Appl. Polym. Sci.* **2014**, *131*, 40473.
17. Liu, L. K.; Cao, Y.; Ma, P. F.; Qiu, C. X.; Xu, W. Z.; Liu, H.; Huang, W. H. *RSC Adv.* **2014**, *4*, 605.
18. Rong, F.; Li, P. *High Perform. Polym.* **2011**, *23*, 585.
19. Xu, X. Y. *Microchim. Acta* **2012**, *176*, 23.
20. Haupt, K.; Linares, A. V.; Linares, M.; Bernadette, T. S. B. *Top. Curr. Chem.* **2012**, *325*, 1.
21. Shen, X. T.; Xu, C. G.; Ye, L. *Ind. Eng. Chem. Res.* **2013**, *52*, 13890.
22. Fang, L. J.; Fang, S. J.; Guo, X. Z.; Zhang, Y.; Zhang, H. Q. *Langmuir* **2012**, *28*, 9767.
23. Tan, C. J.; Tan, Y. W. *Anal. Bioanal. Chem.* **2007**, *389*, 369.
24. Schirhagl, R.; Ren, K. N.; Zare, R. N. *Sci. China Chem.* **2012**, *55*, 469.
25. Li, S. J.; Li, S.; Gong, S. Q. *J. Polym. Sci. Part A: Polym. Chem.* **2009**, *47*, 2352.
26. Xu, L. C.; Pan, J. M.; Pan, J. D.; Li, X. X.; Hang, H.; Cao, Z. J.; Yan, Y. S.; **2012**, *233*, 48.
27. Qin, L.; He, X. W.; Yuan, X.; Li, W. Y.; Zhang, Y. K. *Anal. Bioanal. Chem.* **2011**, *399*, 3375.
28. Qin, L.; He, X. W.; Jia, M.; Li, W. Y.; Zhang, Y. K. *Chem. Eur. J.* **2011**, *17*, 1696.
29. Pan, G. Q.; Zhang, Y.; Guo, X. Z.; Li, C. X.; Zhang, H. Q. *Biosens. Bioelectron.* **2010**, *26*, 976.
30. Adrus, N.; Ulbricht, M. *Polymer* **2012**, *53*, 4359.
31. He, J. X.; Wang, S.; Fang, G. Z.; Zhu, H. P.; Zhang, Y. *J. Agr. Food Chem.* **2008**, *56*, 2919.
32. de Prada, A. G.-V.; Reviejo, A. J.; Pingarron, J. M. *J. Pharm. Biomed.* **2006**, *40*, 281.
33. Guo, L. Y.; Jiang, X. M.; Yang, C. L.; Zhang, H. X. *Anal. Bioanal. Chem.* **2008**, *391*, 2291.
34. Gao, R. X.; Zhang, J. J.; He, X. W.; Chen, L. X.; Zhang, Y. K. *Anal. Bioanal. Chem.* **2010**, *398*, 451.
35. Sun, N.; Wu, S. L.; Chen, H. X.; Zheng, D. J.; Xu, J. W.; Ye, Y. *Microchim. Acta* **2012**, *179*, 33.
36. Kong, X.; Gao, R. X.; He, X. W.; Chen, L. X.; Zhang, Y. K. *J. Chromatogr. A* **2012**, *1245*, 8.
37. Nicholls, I. A.; Andersson, H. S.; Charlton, C.; Henschel, H.; Karlsson, B. C. G.; Karlsson, J. G.; O'Mahony, J.; Rosengren, A. M.; Rosengren, K. L.; Wikman, S. *Biosens. Bioelectron.* **2009**, *25*, 543.
38. Pan, G. Q.; Guo, Q. P.; Ma, Y.; Yang, H. L.; Li, B. *Angew. Chem. Int. Ed.* **2013**, *52*, 6907.
39. Duan, Y. P.; Dai, C. M.; Zhang, Y. L.; Chen, L. *Anal. Chim. Acta* **2013**, *758*, 93.
40. Li, S. J.; Pilla, S.; Gong, S. Q. *J. Polym. Sci. Pol. Chem.* **2009**, *47*, 2352.
41. Liu, X. Y.; Zhou, T.; Du, Z. W.; Wei, Z.; Zhang, J. H. *Soft Matter* **2011**, *7*, 1986.
42. Lagergren, S. *Handlingar* **1898**, *24*, 1.
43. Gosset, T.; Trancart, J. L.; Trancart, D. R. *Water Res.* **1986**, *20*, 21.
44. Chien, S. H.; Chien, W. R. *Soil Sci. Soc. Am. J.* **1980**, *44*, 265.
45. Langmuir, I. *J. Am. Chem. Soc.* **1918**, *40*, 1361.
46. Freundlich, H. M. F. *J. Phys. Chem.* **1906**, *57*, 385.
47. Sips, R. *J. Chem. Phys.* **1948**, *16*, 490.
48. Suedee, R.; Seechamnanturakit, V.; Canyuk, B.; Ovatlarnporn, C.; Martin, G. P. *J. Chroma. A* **2006**, *1114*, 239.